View metadata, citation and similar papers at core.ac.uk
brought to you by CORE
provided by CiteSeerX

COMPRESSION TESTING OF LAMINATES OPTIMISED FOR DAMAGE TOLERANCE

A. T. Rhead, R. Butler and N. Baker
Department of Mechanical Engineering, University of Bath, Bath, UK
R.Butler@bath.ac.uk

SUMMARY

Barely Visible Impact Damage (BVID) can occur when laminated composite material is subject to out-of-plane impact loads and can result in a significant reduction in compressive strength. This paper will report on compression testing of laminates optimised to maximise damage tolerance. Results show an increase of up to 29% in Compression After Impact (CAI) strength in comparison to a baseline configuration.

Keywords: Static strength, Delamination, Compression, Impact.

INTRODUCTION

Carbon fibre reinforced plastics (CFRP) are becoming the material of choice for aircraft designers. As has been popularly reported for a number of years, CFRP has the potential to radically reduce the weight of any vehicle in which it is employed. However, this weight saving is not being fully realised even in the most recent aircraft such as the Boeing 787 and the Airbus A380. There are a number of reasons for this; one of the most significant being Barely Visible Impact Damage (BVID) and the conservative regulations relating to its in service management.

When layered structures are impacted delaminations can occur which can reduce static strength by as much as 60%. Due to the difficulty inherent in detecting BVID, regulations for aircraft manufacture effectively state that it must be assumed that BVID is present everywhere and that the structure must tolerate this damage without failing. As a consequence designs assume conservative strain allowables. A computationally efficient mathematical model (hereafter referred to as the initiation model) has been derived in [1, 2] that uses a simple approximation of BVID morphology and energy considerations to calculate accurately and yet conservatively (and hence safely) the threshold strain below which initiation of damage propagation does not occur. This threshold strain is taken as a lower bound to the compressive strength of simple composite structures containing BVID. The initiation model has been applied successfully to a variety of problems from the literature, see [2]. In [1] an analysis of the model, briefly discussed in Section 2, revealed certain laminate properties that would be desirable for damage tolerant structures.

This paper will focus on a recent series of experiments on two particular stacking sequences that have been optimised based on principles derived in the analysis mentioned above. These laminates, together with a control coupon were impacted and then loaded in compression until failure. Results of these experiments indicate large increases in static strength can be produced and that the model is capable of making qualitative predictions about the compression after impact (CAI) strength of composite laminates. Detailed C-scan information collected during the course of these experiments has allowed an improved representation of BVID to be employed which

has improved accuracy in comparison to the initial approximation to damage morphology.

COMPRESSION AFTER IMPACT MODELLING

A brief derivation of the model, including the key assumptions, equations and concepts, is given here. Full derivations are available elsewhere [1, 2]. The model calculates the threshold strain ε_{th} below which propagation of the delamination damage will not initiate. The central concept of the derivation is to find the difference in energy in the post-buckled sublaminate immediately before, Fig. 1 (a), and after, Fig. 1 (b), the growth of a delamination and to compare this difference to the Mode I fracture energy required to create a new unit of delamination. If sufficient energy is available then a new unit of delamination is created and propagation of the delamination will occur. A thin-film assumption is made that has the effect of allowing no energy to be released from the lower unbuckled region of Figs. 1 (a) and (b). Note that l is the length of the sublaminate immediately before propagation, and δl is an infinitesimal length associated with the length change due to propagation.

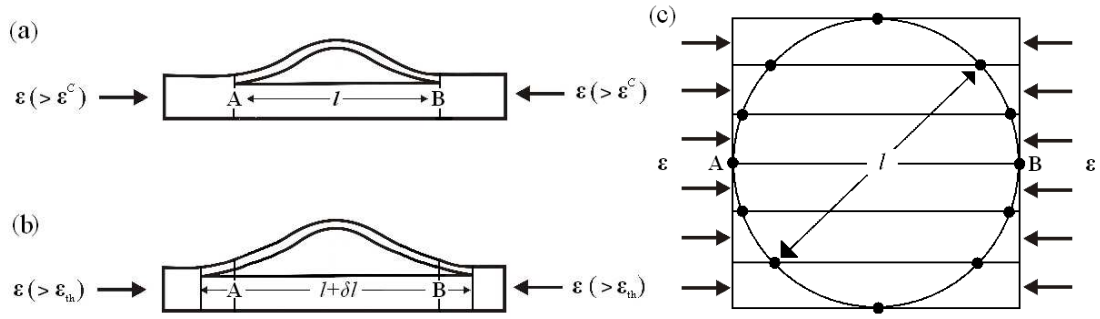

Fig. 1. Thin film model showing; (a) post buckled central section through AB, (b) propagated central section (c), plan view of circular delaminated plate of diameter l with nodes and strips to illustrate VICONOPT discretisation.

The model requires the calculation of the buckling strain ε^C of a delaminated circular region which is dependent on establishing an approximation to the complex damage morphology resulting from BVID. The model is applied at each possible interface in turn up to a depth of 20% of the total thickness away from the face of the laminate. At each application it is assumed that only the delamination being examined is present in the laminate. Each delamination is approximated by a circle, see Fig. 1(c), with individual delamination diameters being calculated using either of the following two damage models. In the Linear Damage Model (LDM), see Fig. 2 and [2], diameters are scaled linearly to a maximum delamination diameter $l_{\max}$ (determined from C-scan data, and occurring at approximately 20% of laminate thickness) from l_b, a diameter computed from the tup diameter using,

$$l_b = \frac{7d}{12} \tag{1}$$

where d is the diameter of the tup used to impact the laminate, at the non-impact face. Whereas the Experimental Damage Model (EDM) uses accurate C-scan information to provide more precise delamination diameters for each interface. In particular, the largest delamination is placed at the correct level which can produce improvements in accuracy. (Note though that the EDM can be conservative as individual delamination diameters are chosen so as to contain the full area of

delamination within a circle. This can result in a much larger circular area than a C-scan image of the damage suggests which can lead to reduced delamination buckling strains).

Having established a set distribution of damage diameters the process of calculating ε^C is completed using the composite buckling program VICONOPT [3]. In essence, the delaminated plate is modelled as a thin film such that the plate boundary along the circular perimeter of the delamination is assumed to be clamped. To obtain ε^C, VICONOPT uses the loadings placed on the thin film by axial compression of the full laminate.

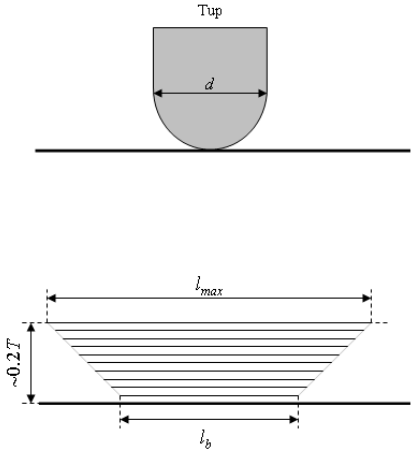

Fig. 2. LDM model of through thickness damage diameter distribution

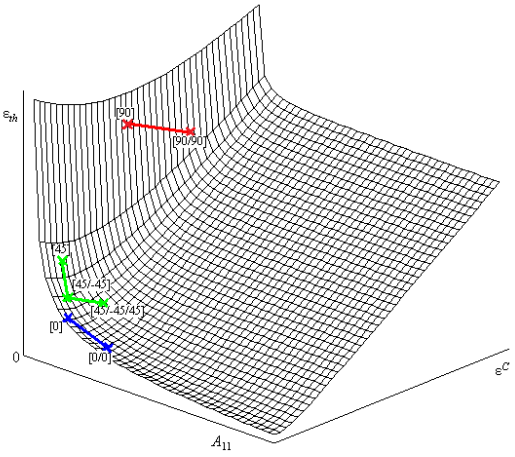

Fig. 3. 3D surface created by fixing $G_I = G_{IC}$. Also plotted are five sub-laminates made from AS4/8552 material.

The program models the plate as a series of finite strips, the edges of which are constrained by nodes approximating a circular boundary, see Fig. 1(c). For the results presented later, 6 equal width strips were used with 12 constrained nodes at the junction of these strips and the circular boundary (for the effect of altering number of strips, nodes and constraints see [2]). Here, constrained implies that no buckling displacement or rotation is allowed at the nodes, thus approximating a fully clamped boundary. It should be noted that VICONOPT buckling analysis is fully general and can analyse the complex unbalanced and asymmetric sublaminates that can arise in the delaminated sublaminate.

The sublaminate, i.e., the thin buckled region in Figs. 1 (a) and (b), is considered to contain bending energy and membrane energy. In order to calculate the energy due to bending it is assumed that the energy stored exactly equals the applied in-plane energy [4]. Hence the application of a simple work done equation gives,

$$U_1(l) = A_{11} l(\varepsilon - \varepsilon^C)\varepsilon^C \tag{2}$$

Note here that ε is the applied strain under displacement control and A_{11} is the axial stiffness of the sublaminate. Note also that the term $(\varepsilon - \varepsilon^C)$ implies bending energy is not stored in the sublaminate until after buckling has occurred.

Following [4, p.171] a simplified membrane energy associated with the sublaminate before buckling occurs is given by,

$$U_2(l) = \frac{A_{11}}{2} l(\varepsilon^C)^2 \tag{3}$$

The above equations describe the energy available in the sublaminate prior to propagation. However, energy for propagation is also available in the form of membrane energy released from the section of the sublaminate of length δl which becomes delaminated during propagation. This energy is calculated using,

$$U_2^* = \frac{A_{11}}{2} \int_0^{\delta l} \varepsilon^2 dx \tag{4}$$

The bending and membrane energy in the sublaminate immediately after propagation occurs can be calculated by replacing l with $l + \delta l$ in Eqs. (2) and (3). Finally, it remains to compare energies before and after propagation to determine whether there is sufficient energy to cause propagation. Eq. (4) and a comparison of buckling strains before and after propagation are employed to give this comparison at the instant propagation occurs. Here G_I is the Mode I strain energy release rate (SERR).

$$G_I = \lim_{\delta l \to 0} \{U_1(l) - U_1(l + \delta l) + U_2(l) - U_2(l + \delta l) + U_2^*\} \frac{1}{\delta l} \tag{5}$$

Hence

$$G_I = \frac{A_{11}}{2} (\varepsilon - \varepsilon^C)(\varepsilon + 3\varepsilon^C) \tag{6}$$

By comparing this value to G_{IC}, the SERR required to cause Mode I failure of the resin, it is possible to determine whether propagation will occur for this level of strain. If the above equation is rearranged and G_I is set equal to G_{IC} it is possible to calculate the threshold strain, when $\varepsilon = \varepsilon_{th}$, i.e.

$$\varepsilon_{th} = \varepsilon^C \left(\sqrt{4 + \frac{2G_{1C}}{(\varepsilon^C)^2 A_{11}}} - 1 \right) \tag{7}$$

The sublaminate at which the lowest threshold strain for propagation is determined will be the first to propagate. Note that for simplicity, the assumption is made (see [2]) that propagation initiates under Mode I conditions in the direction of applied strain ε.

Laminate optimisation

The above model is a combination of the four variables ε^C, ε, A_{11} and G_I. As such it describes a 4D surface. Although it is difficult to extract useful information directly from this 4D surface, it is possible to fix one or more of the variables at an appropriate value (usually at $\varepsilon = \varepsilon^{th}$ or $G_I = G_{IC}$) to create 2D or 3D surfaces which are much easier to interpret. Figure 3 shows a 3D surface created by fixing $G_I = G_{IC}$. This surface allows all possible sub-laminates, which are defined by A_{11} and ε^C with regard to the initiation model, to be compared and hence some optimal features to be identified. With the objective of optimising threshold strain, and hence maximising compressive strength after impact (CAI), it is quite clear from Fig. 3 that this can be accomplished principally by minimising A_{11} and secondly by maximising ε^C. Figure 3

shows the position on the surface of 7 theoretical sub-laminates of a quasi-isotropic laminate made from the AS4/8552 material described below. The sub-laminates highlighted on Fig. 3 consisting of 1 layer have equal damage area and as such their associated threshold strains are directly comparable. Noting this, the sub-laminates made from 90^o layers or 45^o layers are obviously more optimal than those made from 0^o layers as the former offer improved A_{11} and ε^C. Using the above, two stacking sequences have been identified as possible candidates for a damage tolerant quasi-isotropic laminate. The first, $[90_3,45,90,-45_3,0,45_3,0_2,-45,0]_S$, was a product of an optimisation routine described in [5] which sought to minimise both angles between plies (to improve damage resistance) and A_{11} while following current design constraints regarding blocking of a maximum of three plies to prevent intraply cracking. The second $[(45,-45)_4,(90,0)_4]_S$ was a product of the authors' experience which mimics current design philosophies for prevention of global buckling (placing 45^o layers to the outside of the laminate) whilst also exploring the damage tolerance properties of this configuration.

EXPERIMENTAL METHOD

Quasi-isotropic coupons were made from Hexcel AS4/8552 pre-preg layers with material properties given in Table 1 and stacking sequences given in Table 2. Samples were cured in an LBBC Quicklock Thermoclave using the Hexcel specified curing cycle. Coupons were tabbed with 1.5mm aluminium plates to provide grip and to prevent crushing at the loading points.

Table 1.
Material properties. *t* is layer thickness.

Material	E_{11} (GPa)	E_{22} (GPa)	G_{12} (GPa)	ν_{12}	*t* (mm)	G_{1C} (J/m^2)
AS4/8552	128.0	10.3	6.0	0.3	0.125	261

The coupons were subjected to 8J single impacts in an Instron Dynatup 9250HV instrumented impact tester. The tup used was hemispherical with 16mm diameter. The extent of BVID was captured using an Ultrasonic Sciences Ltd. C-scan system. Resulting maximum damage diameters l_{max} were 36mm, 37mm, 42.5mm and 42mm for the Control, 45^o Outer, 90^o Outer (1) and 90^o Outer (2) coupons respectively see Fig.5. Axial compressive load was applied under displacement control from an Instron 5585H test machine until failure. Coupons and their end fixtures are described in fig. 3. An anti-buckling guide is used in order to prevent global buckling and to ensure samples failed by damage propagation following delamination buckling.

Table 2.
Stacking sequences for coupons.

Material (Laminate ID)	Lay-up
AS4/8552 (Control)	$[45,0,-45,90]_{4S}$
AS4/8552 (45^o Outer)	$[(45,-45)_4,(90,0)_4]_S$
AS4/8552 (90^o Outer (1)) and (90^o Outer (2))	$[90_3,45,90,-45_3,0,45_3,0_2,-45,0]_S$

Strains were recorded throughout the tests by two pairs of back-to-back strain gauges attached to a HBM 600 Hz Spider 8 data acquisition system. Coupons were covered

in a random speckle pattern to allow capture of buckling modes and final failure images and video using a Limess VIC-3D HS Digital Image Correlation (DIC) system employing Photron Fastcam SA3 cameras capable of 2000 FPS at full resolution, see Fig. 4.

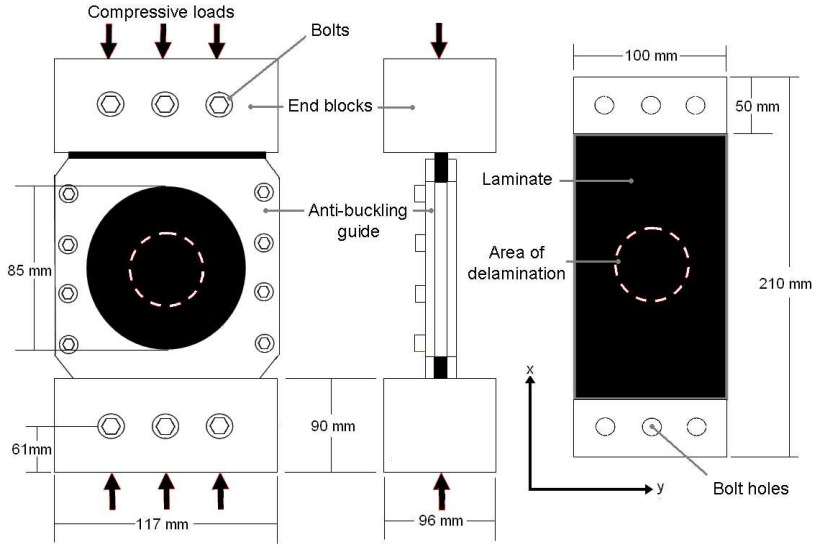

Fig. 3. Experimental set-up and jig.

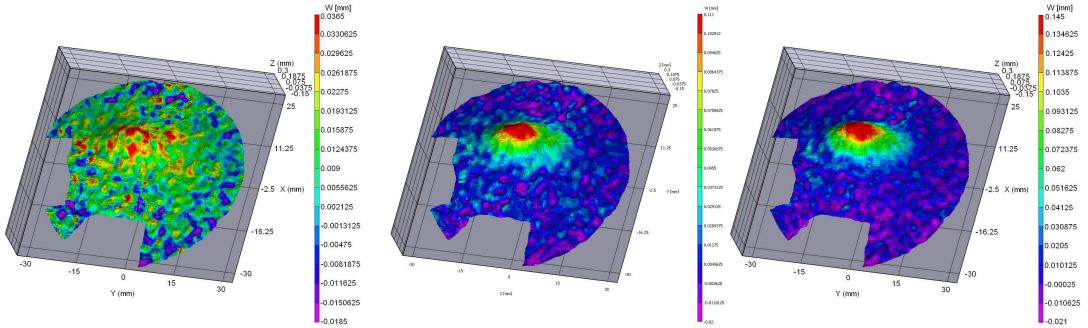

Fig. 4. Three DIC images (1983, 1984 and 1985 of 2726) taken at 50 fps showing displacement contours during delamination buckling of the 90^{o} Outer (2) coupon.

RESULTS

Experimental and analytical failure strains are given together with VICONOPT buckling strains and critical sublaminates in Table 3.

Table 3.

Experimental and analytical VICONOPT buckling and propagation strains for critical sublaminates using the Linear and Experimental Damage Models.

Material (Laminate ID)	Sublaminate Lay-up LDM/EDM	Buckling strain (µstrain) LDM/EDM	Propagation strain (µstrain) LDM/EDM	Experimental
AS4/8552 (Control)	(45,0,-45) / (45,0,-45)	1143 / 3446	3834 / 4742	5700
AS4/8552 (45^{o} Outer)	$(45,-45)_3$ / (45,-45)	4037 / 1904	4997 / 6081	5882
AS4/8552 (90^{o} Outer (1))	$(90_3,45, 90)$* / $(90_3,45)$	6430 / 3014	8238 / 6637	6400
AS4/8552 (90^{o} Outer (2))	$(90_3,45, 90)$* / $(90_3,45)$	6576 / 3086	8349 / 6656	6200

*The LDM actually gives a lower strain at the 5th level but this is disregarded as it occurs at a -45/-45 interface at which (due to fibre bridging) delamination will not occur.

Control Laminate-$[45,0,-45,90]_{4S}$

Figure 5(a) shows the C-scan image before the CAI test with l_{max} = 36mm. Following a divergence in strain at 50-60 kN (see fig. 6(a)) relating to an initial imperfection, contact with the anti-buckling guide occurred between 80-90 kN. Table 3 gives the experimental final failure strain corresponding to a failure load of 107 kN. For the purposes of the EDM the damage diameter at the critical level was 18mm.

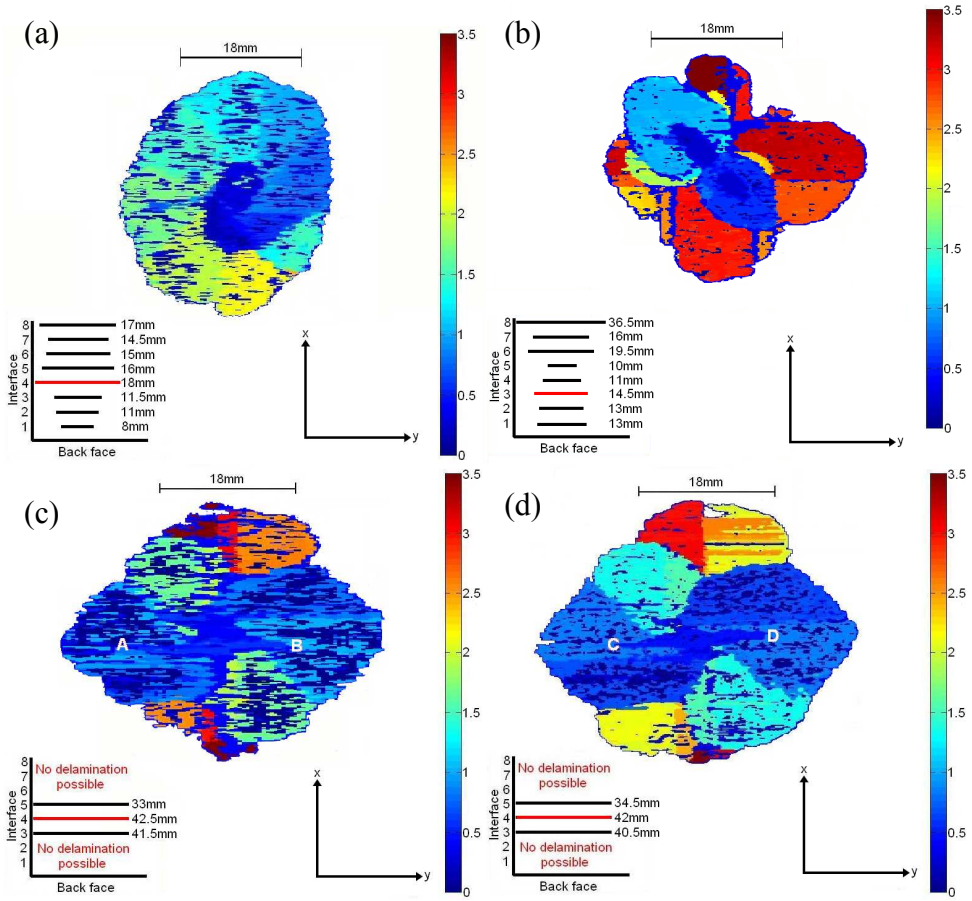

Fig. 5: Ultrasonic C-scan images of BVID with insets showing EDM representations from the non-impact face of (a) the Control , (b) 45° Outer, (c) 90° Outer (1), and (d) 90° Outer (2) coupons. Colour scales relate to through-depth position. Colours toward the top of the scale are closer to the mid-plane of the laminate.

45° Outer Laminate-$[(45,-45)_4,(90,0)_4]_S$

Figure 5(b) shows the C-scan image before the CAI test with l_{max} = 37mm. Table 3 gives the nominal experimental propagation strain corresponding to a failure load of 120 kN. Fig. 6(b) shows that following a divergence in strain at 40-50 kN relating to an initial imperfection, contact with the anti-buckling guide occurred between 70-80 kN. For the purposes of the EDM the damage diameter at the critical level was 14.5mm. Gauges 2 and 4 reach the maximum strain input into the data acquisition system at 107 and 111 kN respectively. Hence the projected average strain from this point (dotted line) is continued with the same gradient. Kinks in gauges 1 and 3 at 120 kN show a damage propagation event. Final failure occurred at 150 kN (equivalent to a nominal strain of 7350 μstrain) due to transverse full width cracking; although post compression C-scan images clearly show damage propagation in the four principal fibre directions.

90^o Outer (1) Laminate-$[90_3,45,90,-45_3,0,45_3,0_2,-45,0]_S$

Figure 5(c) shows the C-scan image before the CAI test with l_{max} = 42.5mm. An intraply crack 3 layers deep, a result of impact, runs from point A to B on Fig. 5 (c) and was a factor in final failure of the laminate. In fig. 6(c) channels 1 and 3 are not considered as part of the average strain because channel 3 appears to be anomalous. Table 3 gives the experimental final failure strain corresponding to a failure load of 119 kN. For the purposes of the EDM the damage diameter at the critical level was 42.5mm.

90^o Outer (2) Laminate-$[90_3,45,90,-45_3,0,45_3,0_2,-45,0]_S$

Figure 5(d) shows the C-scan image before the CAI test with l_{max} = 42mm. An intraply crack 3 layers deep, a result of impact, runs from point C to D on Fig. 5 (d) and was a factor in final failure of the laminate. Table 3 gives the experimental final failure strain corresponding to a failure load of 115 kN as shown in Fig. 6(d). For the purposes of the EDM the damage diameter at the critical level was 42mm. Video from the DIC system indicated delamination buckling occurred (frame 2 Fig. 4) shortly before final failure occurred due to transverse full width cracking.

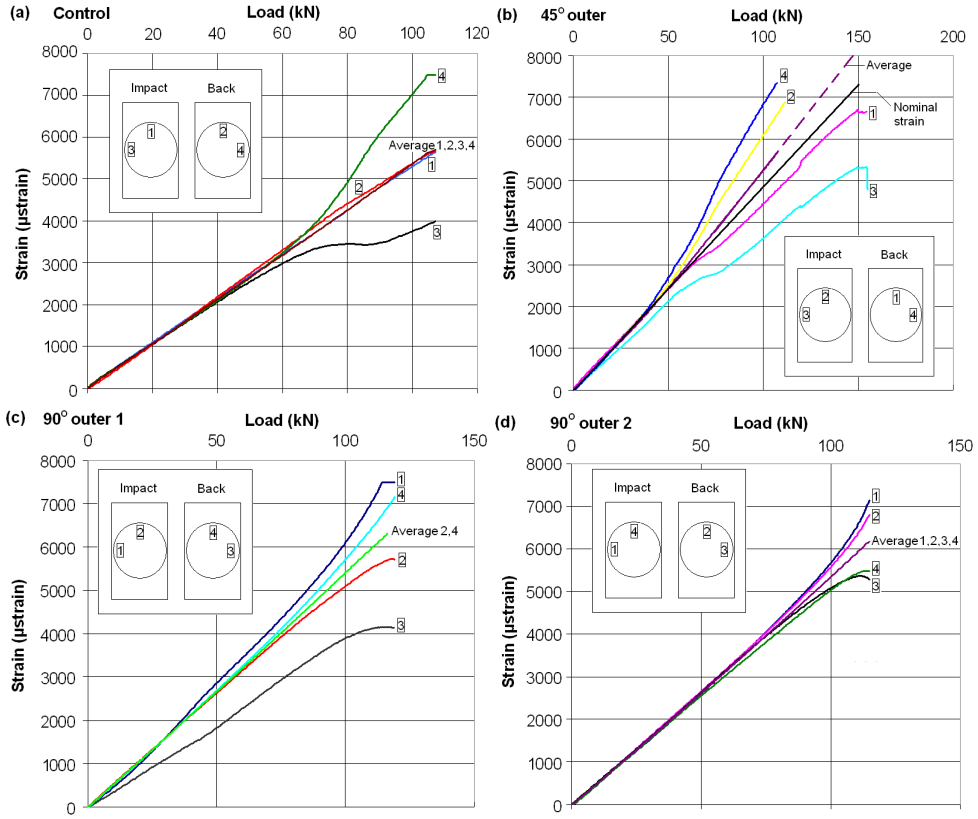

Fig. 6. Strain vs. Load plots for the four coupons with inset showing strain gauge positions: (a) Control, (b) 45^o Outer, (c) 90^o Outer (1) and (d) 90^o Outer (2).

DISCUSSION

Results indicate that all laminates failed as a result of propagation of damage following delamination buckling. The 90^o Outer coupons produced an average improvement in strength over the control laminate of 8% and the 45^o Outer laminate gave improvement in strength of 29%, although propagation occurred at about 8% higher load in comparison to the control. Divergence in strain gauge readings at

medium levels of load for the Control, 45^{o} Outer and 90^{o} Outer (1) coupons is attributed to an initial imperfection leading to bending which is then arrested by contact with the anti-buckling guide as can be seen in Fig. 6.

During the analysis of the C-scans of the 45^{o} Outer coupon it was noted that large delamination damage was not present until the 8th interface, which coincided with the interface of ±45^{o} fibres and 90^{o}/0^{o} fibres. This is an obviously weak interface where stress is likely to be concentrated. It is assumed by the authors that the depth of this weak interface and the fact that a large area of damage was 'drawn' to it away from the critical damage region (approximately 5-20% of laminate thickness) was a major contributing factor to the strength of the overall laminate. Similarly, the stacking sequence for the 90^{o} outer coupons and the C-scan images show an obvious weakness is present between the 4th and 5th layers. However, in contrast to the effect on the 45^{o} Outer coupon, the weak 4th interface in the 90^{o} Outer coupons is thought to have significantly reduced their CAI strength. This may be a factor to consider in future optimisation strategies. Impacts on the 90^{o} Outer laminates produced almost identical damage morphologies as can be seen from Figs. 5(c) and (d). The limited possible interfaces (due to ply blocking) in these coupons at which delamination could occur following impact resulted in impact energy being dispersed over a smaller number of interfaces and hence the area of each delamination had to be larger. Both 90^{o} Outer laminates were also subject to large intraply cracks through the non-impact outer layers which almost certainly had a negative effect on the strength of the laminate.

The LDM analytical results differ from the experimental results by 33%, 32%, 29% and 35% for the Control, 45^{o} Outer, 90^{o} Outer (1) and 90^{o} Outer (2) respectively. Clearly, the LDM does not work well for the more exotic stacking sequences presented here which include blocks of layers with the same orientation and unusual damage morphologies. This is probably due to the inflexibility of the LDM with regard to position of the largest damage diameter. This weakness in damage morphology modelling was exploited by the optimisation procedure to derive optimised laminates. The performance of the 90^{o} Outer coupons could also have been affected by the ASTM standard rectangular impact test window over which coupons were placed during impact. The rectangular shape reduced the length over which 90^{o} fibres bent during impact which in turn increased their bending stiffness when compared to the 0^{o} fibres. This may have caused larger delaminations than assumed by the LDM (and would probably occur in service) to occur closer to the back face (where bending forces peak during impact) thus resulting in an earlier failure than if impact had been over a square window.

However, results can be improved by careful study of the C-scan images to derive the correct damage diameter for each interface see Fig. 5. Results for initial propagation using the EDM differ by 17%, 2%, 4% and 7% for the Control, 45^{o} Outer, 90^{o} Outer (1) and 90^{o} Outer (2) laminates respectively. However, the EDM analysis using the C-scan data was able to capture particularly well the events up to and including failure in the 45^{o} Outer compression test. Note that analysis in [1] shows delamination growth to be stable if the inequality $3\varepsilon^{c} < \varepsilon_{th}$ holds. This inequality does indeed hold for the 2nd interface in the 45^{o} Outer coupon which is thought to be linked to the propagation event at 120 kN (a nominal strain of 5882 μstrain) evident as a jump in readings on the load-strain plot. As the growth at the second level is stable it is unlikely to be the cause of final failure hence propagation at other levels needs to be considered. The level with second lowest propagation strain and hence next to

propagate is the unstable 3rd interface with sublaminate lay-up (45,-45,45) which buckles at 5874 μstrain and has a threshold strain of 7198 which differs by only 2% from the experimental failure strain. Similarly, for the control coupon, propagation at the 2nd interface (4310 μstrain) is predicted to be briefly unstable before becoming stable which is then followed by unstable growth at the 3rd interface. Due to the inherent difficulty in accurate sizing individual delamination areas and the effect this has on calculated strains it is quite likely that propagation at the 2nd level is in fact purely stable which would correlate with experimental results.

CONCLUSIONS

Experimental results demonstrate increases of 8% and 29% in damage tolerant strain can be achieved by replacing a standard $[45,0,-45,90]_{4S}$ laminate with $[90_3,45,90,-45_3,0,45_3,0_2,-45,0]_S$ and $[(45,-45)_4,(90,0)_4]_S$ laminates, respectively. However, stable propagation of damage was observed in the laminate with 45^o material outermost. The results also show that the initiation model is capable in its current form of making qualitative predictions about CAI using the Linear Damage Model and so is a legitimate basis for an optimisation routine designed for damage tolerance.

However, the optimised stacking sequences have identified a weakness in the damage modelling. It has been shown that this weakness can be ameliorated by using experimental C-scan data. However, this is clearly not yet a predictive strategy and so is not applicable to an optimisation procedure.

FUTURE WORK

Future work will centre around an improved optimisation procedure for damage tolerant laminates based on the initiation model. To this end a more detailed predictive method for damage morphology may be necessary though it would need to be computationally efficient to maintain the advantage offered by the current methodology. This may be accomplished by producing a method that can identify weak interfaces and/or cause them to occur deeper in the laminate. Modelling and experimental work is also currently been undertaken on edge impact of stiffeners.

ACKNOWLEDGEMENTS

Andrew Rhead is sponsored by the Great Western Research (GWR) alliance and Airbus UK. The authors are grateful to the University of Bristol for providing materials and Mr. M. Kinawy at the University of Bath for his assistance.

REFERENCES

[1] Rhead AT, Butler, R, Hunt, GW. *Post-buckled propagation model for compressive fatigue of impact damaged laminates*. International Journal of Solids and Structures 2008:45(16):4349-4361.

[2] Rhead AT, Butler R. *Compressive static strength model for impact damaged laminates*. Compos Sci Technol. 2009, doi:10.1016/j.compscitech.2009.01.010.

[3] Anderson MS, Kennedy D. *Transverse shear deformation in exact buckling and vibration of plate assemblies*. AIAA 1991:31(10):1963-1965.

[4] Thompson JMT, Hunt GW. Elastic Instability Phenomena. 1st edition, Wiley and Sons, 1984.

[5] Baker N, Rhead AT, Butler R. *Optimisation of aerospace laminates for damage tolerance.* 7th ASMO-UK/ISSMO international conference of engineering design optimisation, 2008.